

01,08

## Sink strengths and bias factors of voids in BCC metals Fe and V

© A.B. Sivak<sup>1</sup>, V.M. Chernov<sup>2</sup>

<sup>1</sup> National Research Center, „Kurchatov Institute“,  
Moscow, Russia

<sup>2</sup> Advanced Research Institute of Inorganic Materials named after Academician A.A. Bochvar,  
Moscow, Russia

E-mail: Sivak\_AB@nrcki.ru, nrcki@nrcki.ru

Received January 16 2025

Revised January 28, 2025

Accepted January 29, 2025

For bcc metals Fe and V, the most energetically favorable facet patterns of voids have been determined. Their sink strengths for self-point defects (vacancies and self-interstitial atoms) and the bias factors (relative difference in the sink strengths for self-interstitial atoms and vacancies) have been calculated. The calculations have been performed for the range of temperatures 293–1000 K and the void sizes  $2.4-99a$  ( $a$  —  $a$  is the lattice parameter) by an object kinetic Monte Carlo method. Elastic interaction of self-point defects in stable and saddle-point configurations (elastic dipoles) with the elastic fields of voids has been calculated by means of the anisotropic theory of elasticity. Elastic fields of voids have been calculated from atomic displacements from the positions of ideal crystalline lattice sites determined using the molecular statics method. The void bias factor depends on their size and temperature. The bias factor can take values comparable to screw dislocation bias factor values for small voids (sizes are less than several tens of  $a$ ). The results obtained explain the experimentally observed features of radiation swelling of pure iron and vanadium irradiated with neutrons in fast reactors.

**Keywords:** iron, vanadium, voids, sink strengths, bias factors.

DOI: 10.61011/PSS.2025.03.60868.12-25

### 1. Introduction

Traditional theory of radiation-induced metal swelling [1–3] explains the growth of vacancy voids in metals exposed to radiation by the dislocation bias (relative differences of sink strengths for interstitial atoms and vacancies) to self interstitial atoms (SIAs) leading to a dislocation climb due to the prevailing SIA inflow to the dislocations and, consequently, to void growth due to the prevailing vacancy inflow to the voids. Voids, as dislocations, also may have their bias that is usually considered small compared with the dislocation bias for sufficiently large voids. Therefore, the void bias is either neglected or its effect is included in the dislocation bias. It is shown in [4] that such approach leads to highly underestimated role of the void bias in the radiation-induced void assembly evolution that is defined by the void bias to the same degree as by the dislocation bias. Therefore, for modelling of the radiation-induced microstructure evolution, it is important to know the dependences of void bias factors on void size, concentration and temperature. It is still important to determine the bias factors of various microstructure elements because it is difficult to determine them quite accurately by theoretical or experimental methods [5]. Therefore, this problem is solved using multiscale modelling approach through various combinations of computer simulation and theoretical methods. Accuracy and validity of the findings is determined by physical validity of the chosen approaches.

Interaction between voids and self-point defects (SPDs — vacancies, SIAs) away from the void surface (more than the lattice parameter  $a$ ) takes place due to the void-induced elastic field, with which point defects interact as elastic dipoles, thus, leading to anisotropic diffusion of point defects in the void neighborhood. Diffusion anisotropy is determined only by the interaction between the elastic field and saddle-point configurations of point defects [6,7] and this type of interactions makes a decisive contribution to the magnitude of void bias factor [7].

Sink strengths and bias factors of spherical voids are calculated in [7–10] taking into account the effects of anisotropic diffusion of point defects in elastic fields induced due to the difference in symmetry of the saddle-point configuration of point defects from the spherical one. Sink strengths of voids in [7] are determined by solving diffusion equations in [8] using the object kinetic Monte Carlo (OKMC) method, in [9] using a non-stochastic method based on the absorbing Markov chain theory, in [10] using a phase field method. In [7–10], elastic fields of voids are determined using the Eshelby solutions [11,12] for spherical inclusions in an elastic isotropic [7–9] and elastic anisotropic [10] media that differs both quantitatively and qualitatively from a molecular static (MS) solution that takes into account an atomistic surface configuration of voids [13,14]. In [15–17], the bias factor of spherical voids is determined through the difference of effective void sizes for vacancies and SIAs using a criterion of exceedance of a voluntary chosen threshold for the binding energy of voids

with vacancies and SIAs. Energy of interaction between voids and point defects is determined using the MS method to ensure the most correct currently available determination. However, the interaction is calculated only for point defects (and their small clusters in [17]) in stable configurations. Thus, the most important effect (interaction with saddle-point configurations of point defects) that determines the bias factor is not considered in [15–17]. Some of the evaluations listed above give high values for the bias factor of small-size voids (tens of percent), and all above-mentioned works note that the bias factor decreases as the void size increases.

This study uses the MS calculations to determine the most energetically favorable void faceting in body-centered cubic (BCC) Fe and V metal crystals. These metals are of high research and practical interest, as they are used as the basis for development of structural steels and alloys for nuclear and thermonuclear energy reactors [18]. Then, sink strengths for SPDs and bias factor (void size range  $2\text{--}99a$  and temperature range  $293\text{--}1200\text{ K}$ ) are calculated for voids with the most energetically favorable faceting using the multiscale approach. Within this approach, the anisotropic SPD diffusion in void elastic fields determined by the MS method is simulated by the OKMC method [19]. Interaction between the elastic fields of voids and SPDs treated as elastic dipoles is calculated within the anisotropic elasticity theory.

## 2. Models and calculation methods

### 2.1. Atomistic models of the studied types of voids

Faceted void formation energy  $E^F$  can be calculated to a first approximation as a sum of products of facet areas by the corresponding surface energies  $\gamma$ . If  $\gamma$  were independent of the surface orientation, then spherical voids would have the lowest  $E^F$ , because such voids have the smallest surface area with fixed volume. However,  $\gamma$  in metals is an anisotropic quantity due to the crystal structure of metals. Consequently,  $E^F$  of faceted voids can be hypothetically lower than that of spherical voids. Evaluation of  $\gamma$  for BCC metals using the broken bond model [20] (bonds between the 1st and 2nd nearest neighbors) showed that the  $\{110\}$ ,  $\{100\}$ ,  $\{211\}$ ,  $\{111\}$  surfaces had the lowest values of  $\gamma$  in ascending order. Therefore, to determine the most energetically favorable faceting, the size dependences of the formation energy of the following types of voids are calculated in the work:

- spherical voids (S);
- cube with the  $\{100\}$  facets ( $C_{100}$ );
- octahedron and rhombic dodecahedron with the  $\{110\}$  facets ( $O_{110}$  and  $R_{110}$ );
- regular octahedron with the  $\{111\}$  facets ( $O_{111}$ );
- deltoidal icositetrahedron with the  $\{211\}$  facets ( $D_{211}$ ).

Figure 1 shows voids representing each of the above types. Voids are visualized by imaging the atoms on their

**Table 1.** Geometric relations for the given types of pores

Type of void	$b, V^{1/3}$	$S, b^2$	$S(n)/n^{2/3}, a^2$
$C_{100}$	1	6	$2^{1/3}3 \approx 3.77976$
$O_{111}$	$3^{1/3}/2^{1/6}$	$2 \cdot 3^{1/2}$	$3^{7/6} \approx 3.60281$
$O_{110}$	$3^{1/3}$	$2^{3/2}$	$2^{5/6}3^{2/3} \approx 3.70629$
$R_{110}$	$3^{1/2}/2^{4/3}$	$2^{7/2}$	$2^{1/6}3 \approx 3.36739$
$D_{211}$	$(122 + 71\sqrt{2})^{-1/6}$	$6\sqrt{29-2^{3/2}}$	$\frac{\sqrt{29-2^{3/2}}}{\sqrt[3]{61+71/2^{1/2}}} 3 \approx 3.19150$
S	–	–	$\pi^{1/3}3^{2/3} \approx 3.04647$

surfaces (atoms with coordination number lower than 14 — the sum of eight first and six second nearest neighbors in the BCC lattice). Different colors of atoms reflect different coordination numbers: cyan for 7, yellow for 8, red for 9, orange for 10, violet for 11, blue for 12, green for 13. With such void visualization method, each type of facet has its typical pattern. The  $\{100\}$  type void facets consist of two planes of red and green atoms (Figure 1, *a*),  $\{110\}$  facets consist of one plane of orange atoms (Figure 1, *b, c*),  $\{111\}$  facets consist of three planes of cyan, orange and green atoms (Figure 1, *d*),  $\{211\}$  facets consist of two planes of yellow and blue atoms (Figure 1, *e*). Spherical voids actually consist of a set of  $\{100\}$ ,  $\{110\}$ ,  $\{111\}$  and  $\{211\}$  planes — their typical patterns can be seen clearly in Figure 1, *f*.

Table 1 summarizes geometrical relations, that are useful for further discussion, for the given types of voids to link the void volume  $V$ , surface area  $S$ , facet edge length  $b$  and the number of vacant lattice sites  $n$  in voids. Void volume equal to  $V = n\Omega = na^3/2$  is assumed throughout the paper.

For ease of comparing the properties of different types of voids, the effective void diameter is introduced:

$$d_{\text{eff}}(n) = (6/\pi)^{1/3}V^{1/3} = (3/\pi)^{1/3}n^{1/3}a. \quad (1)$$

### 2.2. MS model for calculating void properties and elastic fields

Energy characteristics of spherical vacancy voids with diameter  $d = 2\text{--}20a$  and their elastic fields were determined in [14] by the MS method using interatomic interaction potentials (IIP) M07 for Fe [21] and for V [22]. These IIP describe the volumetric and surface properties of crystals sufficiently accurately. Similar calculations for spherical voids with  $d = 30\text{--}100a$  and for faceted voids with  $d_{\text{eff}} = 3\text{--}100a$  are conducted in this work using the same procedure and the same IIP as in [14].

Atomistic configuration corresponding to a void within the material is formed by removing atoms inside a sphere or polyhedron with a preset size from a model cubic crystallite with size  $L$  (the center of the void is in the

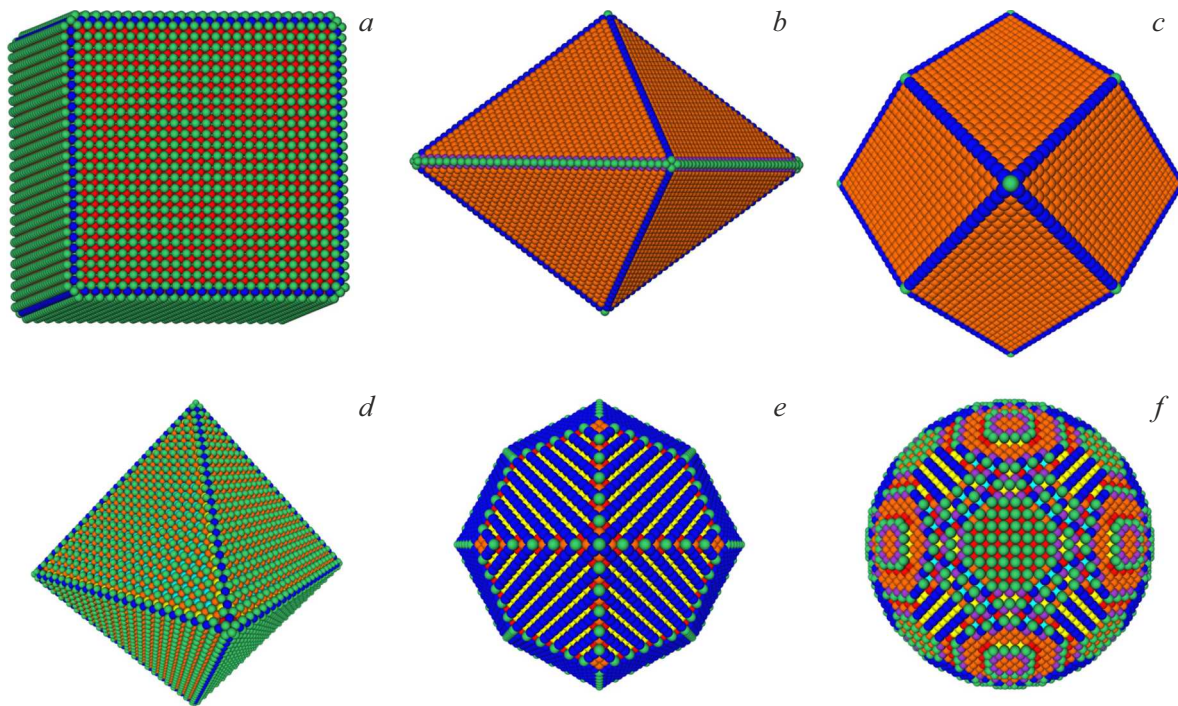


**Figure 1.** View of the surface atoms of voids with different shapes and with size  $\sim 30a$ : *a* — cube with the facets  $\{100\}$  ( $C_{100}$ ); *b* — octahedron with the facets  $\{110\}$  ( $O_{110}$ ); *c* — rhombic dodecahedron with the  $\{110\}$  ( $R_{110}$ ); *d* — octahedron with the facets  $\{111\}$  ( $O_{111}$ ); *e* — deltoidal icositetrahedron with the facets  $\{211\}$  ( $D_{211}$ ); *f* — sphere (S).

center of the crystallite) with rigid boundary conditions followed by minimization of the crystallite's potential energy by the gradient descent method. Minimization is carried out until the maximum force acting on atoms becomes lower than  $10^{-9}$  eV/nm. In [14], a limiting value of  $10^{-7}$  eV/nm was used, but this value is reduced by two orders of magnitude in this work due to much larger crystallite sizes (maximum  $L$  in this work and in [14] is equal to  $225a$  and  $100a$ , respectively) in order to keep the same level of calculation accuracy as in [14].  $L$  is chosen such as the boundary conditions do not exert any noticeable effect on the properties to be calculated (Table 2).

### 2.3. OKMC model for calculating sink strengths of voids

Computational cell for OKMC calculations is a cube with side  $L^{MC}$  with a void in its center. Periodic boundary conditions are imposed on the facets of the computational cell. Thus, an equispaced cubic lattice of voids of the same size with concentration  $N_V = (L^{MC})^{-3}$  is simulated. The presence of space correlation of the void arrangement has no any significant effect on the results of sink strength calculations when the absorbed defects have a three-dimensional migration mechanism [23].

Initial positions of defects are set randomly in the cell bulk, excluding a region within the void. The initial coordinates of defects are a discrete set coinciding with BCC lattice sites. Defects jump into the nearest sites

in accordance with their diffusion mechanism: vacancies can move into any of 8 nearest neighboring sites,  $\langle 110 \rangle$  dumbbell SIA can move into 4 nearest sites with two different finite splitting orientations for each site (Johnson migration mechanism [24]).

Lattice sites with at least one vacant site among the neighboring sites (1-st and 2-nd nearest neighbors of the BCC lattice) are referred to as the surface lattice sites. MS calculations have shown that an SIA recombines spontaneously with a void, if it gets into sites nearest to the surface ones (near-surface sites). MS calculations also have shown that vacancies that fall within the near-surface site layer have much lower migration energy for movement to the surface layer than in other directions. Therefore, the OKMC calculations consider that SIAs and vacancies are absorbed by the void if they enter a near-surface site during migration along the crystal lattice.

To determine the probabilities of defect jumps in different directions, it is necessary to know defect interaction energies in the corresponding saddle-point configurations and, consequently, the elastic field in saddle-point positions. Elastic field created by a void within the material bulk is calculated from the coordinates of atoms shifted from sites of an undeformed crystal lattice determined by the MS method. Within the used procedure [14], the values of the strain tensor are determined only for the lattice sites corresponding to defect positions in the stable states. Therefore, the field for SPD saddle-point positions is calculated by linear interpolation of the strain tensor in

**Table 2.** Sizes of model crystallites  $L$  used for calculating the properties of different types of voids with volume  $V$ . Values of  $V$  for voids whose formation energies and elastic fields were calculated earlier in [14] are italicized

$L, a$	$V, \Omega$					
	$C_{100}$	$O_{111}$	$O_{110}$	$R_{110}$	$D_{211}$	$S$
30	9, 35, 91	15, 57	19, 85	15, 65, 175	65	27, 59
7	189, 341, 559, 2331	143, 1247	231, 489, 891, 1469, 2255, 3281	369, 671, 1105, 1695, 2465	779	137, 229, 1037, 2277
80	–	–	–	3439	3005	3527, 5065
100	9009	8569	8119	7825	7607	8363
120	–	–	–	–	15449	–
150	29449	27455	28595	29679	27395	28325
170	–	–	–	–	–	130869
190	–	–	–	–	–	359253
225	–	–	–	1024255	–	1047139

lattice sites corresponding to the defect position before and after the jump. If the final defect position corresponds to a near-surface (absorbing) site, the field for the corresponding saddle point is determined by linear extrapolation of the strain tensor in lattice sites, one of which corresponds to the defect position before the jump, and the other one is the nearest neighbor of the first site in a direction opposite to the jump direction.

Energies of interaction between SPDs and elastic fields of voids are calculated according to the anisotropic elasticity theory (in [14], it is shown that calculations of void-SPD interaction energy using the elasticity theory agree with the direct MS calculations of this quantity) according to [25,26], as

$$E(\mathbf{r}) = -P_{ij}\varepsilon_{ij}(\mathbf{r}), \quad (2)$$

where  $P_{ij}$  is the dipole tensor of the given SPD configuration,  $\varepsilon_{ij}$  is the strain tensor of the elastic field created by a void in the SPD position  $\mathbf{r}$ .

SIA and vacancy properties (dipole tensors of the stable and saddle-point configurations) that are necessary for calculating the interaction energy were calculated by the MS method in [27] for Fe and in [19] for V. Applicability of IIP R01 in Fe and V used for calculation of their characteristics is justified in [28]. To accelerate the OKMC calculations, elastic interaction between a void and a defect is calculated only in a limited cubic volume with the void in its center. This volume (cube side  $L^{\text{int}}$ ) is selected in such a way that the deviation introduced by this simplification into the calculated sink strengths is lower than the statistic calculation error. The values of  $L^{\text{int}}$  are summarized in Table 3.

There is only one defect in the computational cell during the simulation process. As soon as it is absorbed by the void, the next defect is introduced. The calculation ends when a sufficient number of trajectories for the preset

statistic accuracy level is achieved. The sink strength is defined as follows (see, for example, [29])

$$k^2 = 6\lambda^{-2}\langle N \rangle^{-1}, \quad (3)$$

where  $\lambda$  is the defect jump length (with the given diffusion mechanisms, the defect may make jumps only with one length  $3^{1/2}a/2$  in different directions),  $\langle N \rangle$  is the mean number of defect jumps made before the absorption by the sink.

The void bias factor is defined in this work as

$$D = (k_+^2 - k_-^2)/(k_+^2 + k_-^2), \quad (4)$$

where indices  $+$  and  $-$  are used for SIAs and vacancies, respectively.

To calculate the sink strengths of voids without taking into account elastic interaction between voids and defects ( $k_{0,\pm}^2$ ),  $10^7$  trajectories are calculated, taking into account ( $k_{\pm}^2$ ) —  $10^5$  trajectories. This provides a statistical calculation error of 0.1% and 1%, respectively, with a confidence probability of 99%. Such considerable number of trajectories for calculation of  $k_{0,\pm}^2$  can be simulated due to using the accelerated Monte Carlo method [30] (algorithm 3S). This method is also used for accelerated calculations of  $k_{\pm}^2$  since there is no elastic interaction between defects and voids when defects are far away from voids (a region outside the cube with side  $L^{\text{int}}$ , Table 3).

## 3. Results

### 3.1. Formation energies of voids and surface energies

Figure 2 shows size dependences of the normalized formation energy of different types of voids  $E^F(n)/n^{2/3}$

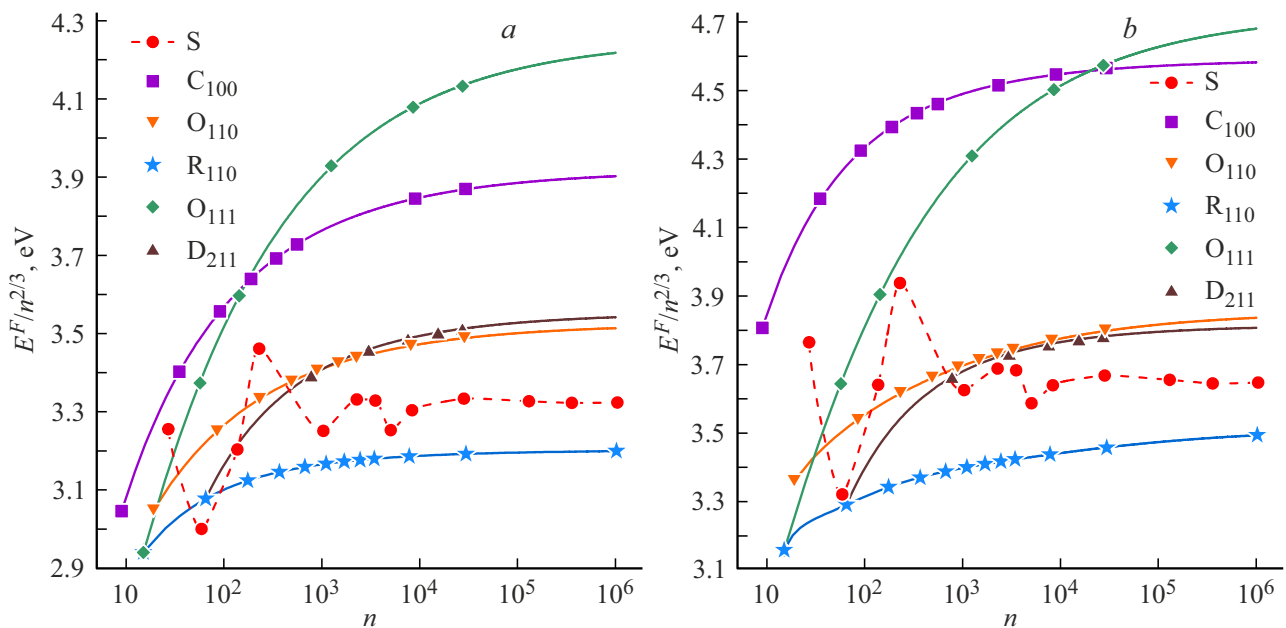


**Figure 2.** Size dependences of normalized formation energy of different types of voids  $E^F(n)/n^{2/3}$  ( $n$  — number of vacant lattice sites in a void):  $a$  — Fe;  $b$  — V. Solid lines — approximation (5).

**Table 3.** Values of  $L^{\text{int}}$  (in  $a$ ) for voids with  $d_{\text{eff}}$  (in  $a$ ) used for the calculations

$d_{\text{eff}}$	2–3	3–6	6–8	8–14	14–17	17–25	25–40	40–60	60–90	> 90
$L^{\text{int}}$	10	24	50	64	74	94	144	160	180	200

in Fe and V. Calculated data (points on curves) for faceted voids are well approximated by a polynomial dependence

$$E^F(n)/n^{2/3} = \gamma_{hkl} S(n)/n^{2/3} + \sum_{i=1}^m a_i n^{-i/3}, \quad (5)$$

Here,  $S(n)/n^{2/3}$  is the geometric factor for a specified faceting (values for different types of voids are given in Table 1);  $\gamma_{hkl}$  is the surface energy of an infinite flat surface  $\{hkl\}$ ;  $\gamma_{hkl}$  and  $a_i$  are the adjustable parameters;  $m = 2$  for all given types of void faceting in Fe and V, excluding  $O_{110}$  ( $m = 3$ ) and  $R_{110}$  ( $m = 5$ ) in V. Formation energies of  $R_{110}$ - and  $O_{111}$ -voids with  $n = 15$  and of  $R_{110}$ - and  $D_{211}$ -voids with  $n = 65$  are the same, because these are the same voids in terms of atomistic approach. These voids may be assigned to one or another faceting class due to approximations used in transition from a real discrete atomistic void surface to continuum void surface interpretation.

The calculated values of  $\gamma_{hkl}$  for Fe and V are summarized in Table 4. Values of  $\gamma_{hkl}$  ( $\{hkl\} = \{100\}$ ,  $\{110\}$  and  $\{111\}$ ) for Fe virtually coincide with those obtained in [21] by the direct MS calculation of free flat surface formation energy using the same interatomic interaction potential as in this work. This agreement verifies the calculations in this work.  $\gamma_{\text{sph}}$  calculated as the ratio of the formation energy of the largest considered spherical void to

its surface area is added in Table 4. The  $\{110\}$  planes have the lowest values of  $\gamma_{hkl}$ .  $E^F(n)/n^{2/3}$  for S-voids are not smooth, however, data scatter in transition between void sizes decreases as  $n$  grows and becomes insignificant at  $n \gtrsim 10^4$  ( $d_{\text{eff}} \gtrsim 20a$ ).

Direct experimental measurement of the metal surface energy at temperatures much lower than the melting temperature is a challenging problem. In [31], based on the concepts of the tight binding approximation, a relation is proposed that links the cohesive energy  $E_{\text{coh}}$  with  $\gamma$  for transition metals. For the  $\{110\}$  surface of BCC metals, this relation is written as

$$\gamma_{110} = 0.134c\sqrt{2}a^{-2}E_{\text{coh}}, \quad (6)$$

where  $c$  is equal to 1 and 1.2 for non-magnetic and magnetic transition metals, respectively. Experimental values of  $E_{\text{coh}}$  are 4.28 and 5.31 eV in Fe and V, respectively [32], whence, using (6), 1.91 and 1.77 J/m<sup>2</sup>, respectively, are obtained for  $\gamma_{110}$ . These values agree well with those obtained in this work (Table 4).

It can be seen from (5) that, when  $n \rightarrow \infty$ , the main contribution to  $E^F$  is given by  $\gamma_{hkl}S$ . Hence and also from the data in Tables 1 and 4 it follows that  $R_{110}$  type faceting is the most energetically favorable for large voids with the same volume in both Fe and V. S-voids are the next in order of favorability. S-void formation energy in the limit of

**Table 4.** Surface energies (in J/m<sup>2</sup>) for the {hkl} surface in Fe and V

Material	$\gamma_{100}$	$\gamma_{110}$	$\gamma_{111}$	$\gamma_{211}$	$\gamma_{\text{sph}}$
Fe	2.037	1.869	2.319	2.188	2.144
V	2.120	1.821	2.290	2.087	2.090

**Table 5.** Sink strengths of R<sub>110</sub>-voids  $I_{0,\pm}^2$  normalized to  $2\pi N_V d_{\text{eff}}$ 

V, $\Omega$	$d_{\text{eff}}, a$	$\frac{k_{0,+}^2}{2\pi N_V d_{\text{eff}}}$	$\frac{k_{0,-}^2}{2\pi N_V d_{\text{eff}}}$	V, $\Omega$	$d_{\text{eff}}, a$	$\frac{k_{0,+}^2}{2\pi N_V d_{\text{eff}}}$	$\frac{k_{0,-}^2}{2\pi N_V d_{\text{eff}}}$
15	2.4	2.048	2.075	1695	12	1.297	1.300
65	4.0	1.675	1.687	2465	13	1.281	1.281
175	5.5	1.508	1.516	3439	15	1.265	1.270
369	7.1	1.416	1.420	7825	20	1.247	1.251
671	8.6	1.361	1.366	29679	30	1.253	1.253
1105	10	1.324	1.326	1024255	99	1.621	1.623

large  $n$  is higher by 4% that of R<sub>110</sub>-voids. With low  $n$  up to  $n = 15$ , R<sub>110</sub> faceting is also most energetically favorable. The only exception is a S-void with  $n = 59$  in Fe, whose formation energy is lower by 2% than that calculated for the R<sub>110</sub>-void in accordance with (5).

Under irradiation (in accelerators and reactors), voids with facets corresponding to low-index lattice planes are often formed in metals, including BCC metals in the form of dodecahedra with the {110} facets and cubes with the {100} facets [33]. Voids in the form of dodecahedra with the {110} facets were observed in V (dose  $3 \cdot 10^{22}$  n/cm<sup>2</sup> at 650 °C [34], dose  $3.6 \cdot 10^{22}$  n/cm<sup>2</sup> at 550 and 600 °C [35]) and Fe (dose  $3 \cdot 10^{21}$  n/cm<sup>2</sup> at 450 °C irradiated in fast reactors [36]). Therefore, the properties of R<sub>110</sub>-voids in Fe and V are of high interest when radiation-induced swelling in reactor neutron irradiation conditions is addressed.

### 3.2. Sink strengths and bias factors of R<sub>110</sub>-voids

Sink strengths of voids for SIAs and vacancies can be conveniently represented in the form of a product of two quantities: sink efficiency  $\xi^\pm$  and sink strength of a void that doesn't interact with a point defect:  $k_{\pm}^2 = \xi^\pm k_{0,\pm}^2$ . It is more convenient to use sink efficiencies than sink strengths because test calculations showed that the former, unlike the latter, weakly depend on the void concentration (computational cell size  $L^{\text{MC}}$  varied from 200 to 600 $a$ ). Magnitudes of  $k_{0,\pm}^2$  depend only on the problem geometry and point defect diffusion mechanism, rather than on material and temperature. Values of  $k_{0,\pm}^2$  normalized to  $2\pi N_V d_{\text{eff}}$  for the R<sub>110</sub>-voids with  $d_{\text{eff}}$  and  $N_V = (400a)^{-3}$  in BCC crystals are summarized in Table 5.

$\xi^\pm(T)$  for R<sub>110</sub>-voids in Fe and V are shown in Figure 3. Dependences are not shown for all void sizes of interest, only for some typical ones, because many dependences are close to each other and hamper perception. These dependences have a different behavior depending on the features of the interaction between the void-induced elastic field and a migrating defect (elastic dipole).

$\xi^+(T)$  in Fe and V for all the considered R<sub>110</sub>-void sizes are characterized by a monotonic decrease with increasing temperature from values  $\xi^+$  higher than 1 to the asymptotic value  $\xi^\pm = 1$  (Figure 3, a, b).  $\xi^+$  takes on its maximum value for voids with 5.5 $a$  at  $T = 293$  K and is equal to 1.43 and 1.47 in Fe and V, respectively.

$\xi^-(T)$  in V for R<sub>110</sub>-voids with  $d_{\text{eff}} < 10a$  have a similar form (Figure 3, d).  $\xi^-$  takes on its maximum value for voids with 7.1 $a$  at  $T = 293$  K and is equal to 1.21.  $\xi^-(T)$  in V for R<sub>110</sub>-voids with  $d_{\text{eff}} > 10a$  become slightly lower than 1 as the temperature grows (Figure 3, d).

$\xi^-(T)$  in Fe for all given void sizes are lower than 1 at all temperatures and tend to 1 with temperature growth. The minimum value of  $\xi^-$  at  $T = 293$  K is equal 0.97 (Figure 3, c).

All dependences in Figure 3 are well described by the following expression

$$\xi(T) = 1 + AT^{-1/2} + B \exp(-CT), \quad (7)$$

where  $A, B, C$  ( $C > 0$ ) are the adjustable parameters.

$\xi^\pm(d_{\text{eff}})$  for R<sub>110</sub>-voids in Fe and V are shown in Figure 4. Except  $\xi^-(d_{\text{eff}})$  in Fe, all other dependences first grow with  $d_{\text{eff}}$  and reach their maximum with  $d_{\text{eff}} \sim 5.5-7.1a$ , and then decrease and approach 1 (Figure 4, a, b, d).  $\xi^-(d_{\text{eff}})$  in Fe weakly depend on the void size and tend asymptotically to 1 in the limit of large sizes (Figure 4, c).

Sink efficiencies of voids are fully determined by the spatial dependence of the energy of interaction between SPDs (elastic dipoles) and void elastic field as described by equation (2). Dipole tensors of vacancies and SIAs in saddle-point configurations have trigonal and monoclinic symmetries, respectively. One saddle point and three saddle points correspond to each jump direction for a vacancy and SIA, respectively. Averaging of three dipole tensors corresponding to these three saddle points gives a tensor with a trigonal symmetry. Utilization of such averaging in diffusion problems is justified [6,7]. In case of trigonal symmetry of tensor  $P_{ij}$ ,  $P_{11} = P_{22} = P_{33} = \text{Tr} P/3$  ( $\text{Tr} P$  is the trace of tensor  $P_{ij}$ ) and  $|P_{23}| = |P_{13}| = |P_{12}| = P_n$  are true in the crystallographic system of coordinates with unit vectors along  $\langle 100 \rangle$  directions. Then equation (2) may be rearranged to the following form

$$E(\mathbf{r}) = -\frac{1}{3} \text{Tr} P \text{Tr} \varepsilon(\mathbf{r}) - 2P_n \sum_{k=1}^3 \varepsilon_k \text{sgn} P_k, \quad (8)$$

where  $\text{Tr} \varepsilon$  is the trace of tensor  $\varepsilon_{ij}$ ,  $\text{sgn}$  is the sign function ( $\text{sgn} x = x/|x|$  at  $x \neq 0$ ,  $\text{sgn} x = 0$  at  $x = 0$ ), and index  $k = 1, 2, 3$  corresponds to a pair of indices  $ij = 23, 13, 12$ .

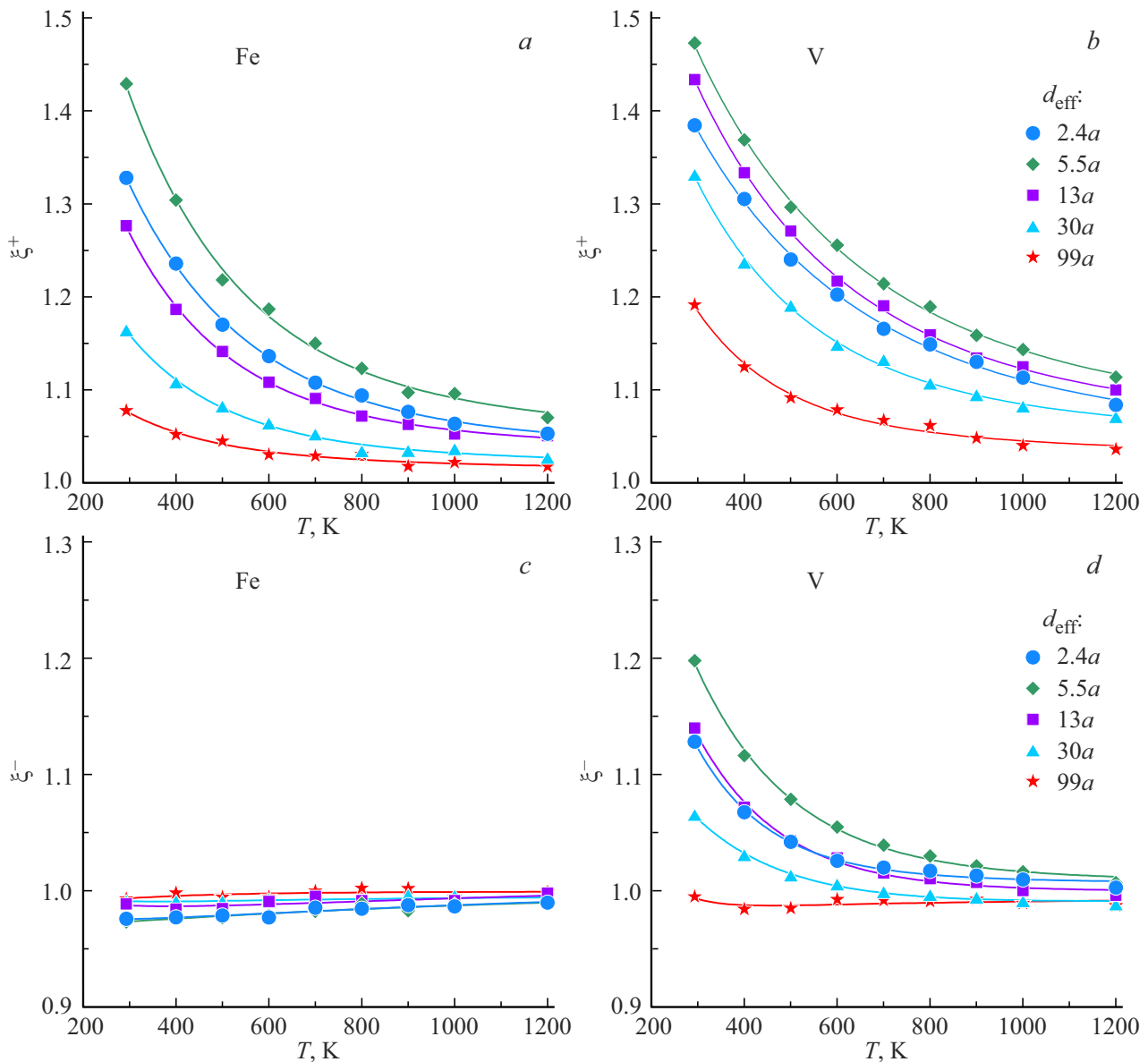


**Figure 3.** Dependences of sink efficiencies of  $R_{110}$ -voids with  $d_{\text{eff}} = 2.4, 5.5, 13, 30, 99a$  for SIAs (a, b) and vacancies (c, d) in Fe (a, c) and V (b, d). Solid lines — approximation (7).

The first and second terms in the right-hand side of (8) describe the parts of interaction defined by volumetric and shear strains, respectively. Eshelby's solution [11,12] for a spherical inclusion in an isotropic medium used in [7–10] to calculate sink strengths of voids gives  $\text{Tr} \varepsilon = 0$ . Consequently, elastic interaction in such approximation is determined only by the second term in (8). Elastic fields induced by voids are calculated in this work by the MS method, i.e. without using the continuous isotropic medium approximations. According to the calculation data, the trace of strain tensor near voids is not equal to zero and reaches 0.6% and 2% in absolute values in Fe and V, respectively, near void surfaces (Figure 5). In some cases, this may lead to a prevailing contribution of the first term of (8) to the interaction energy and, thus, to the dominating role of

void-induced volumetric strains in formation of void sink strengths and bias factors.

For quantitative determination of the effect of the first and second terms in (8) on void sink efficiencies in Fe and V, additional calculations of void sink efficiencies were performed for SPDs at 293 K, where  $\text{Tr} P = 0$  was set for the saddle-point configurations of SPDs, i.e. contribution of the first term (8) to the interaction energy was zeroed. By comparing these values with those obtained when both terms of (8) are taken into account, it was found that consideration of the first term of (8) contributes to deviation of  $\xi$  from 1 equal to:

- 40–50% and 75–80% for SIAs in Fe and V, respectively;
- 40–50% for vacancies in V;

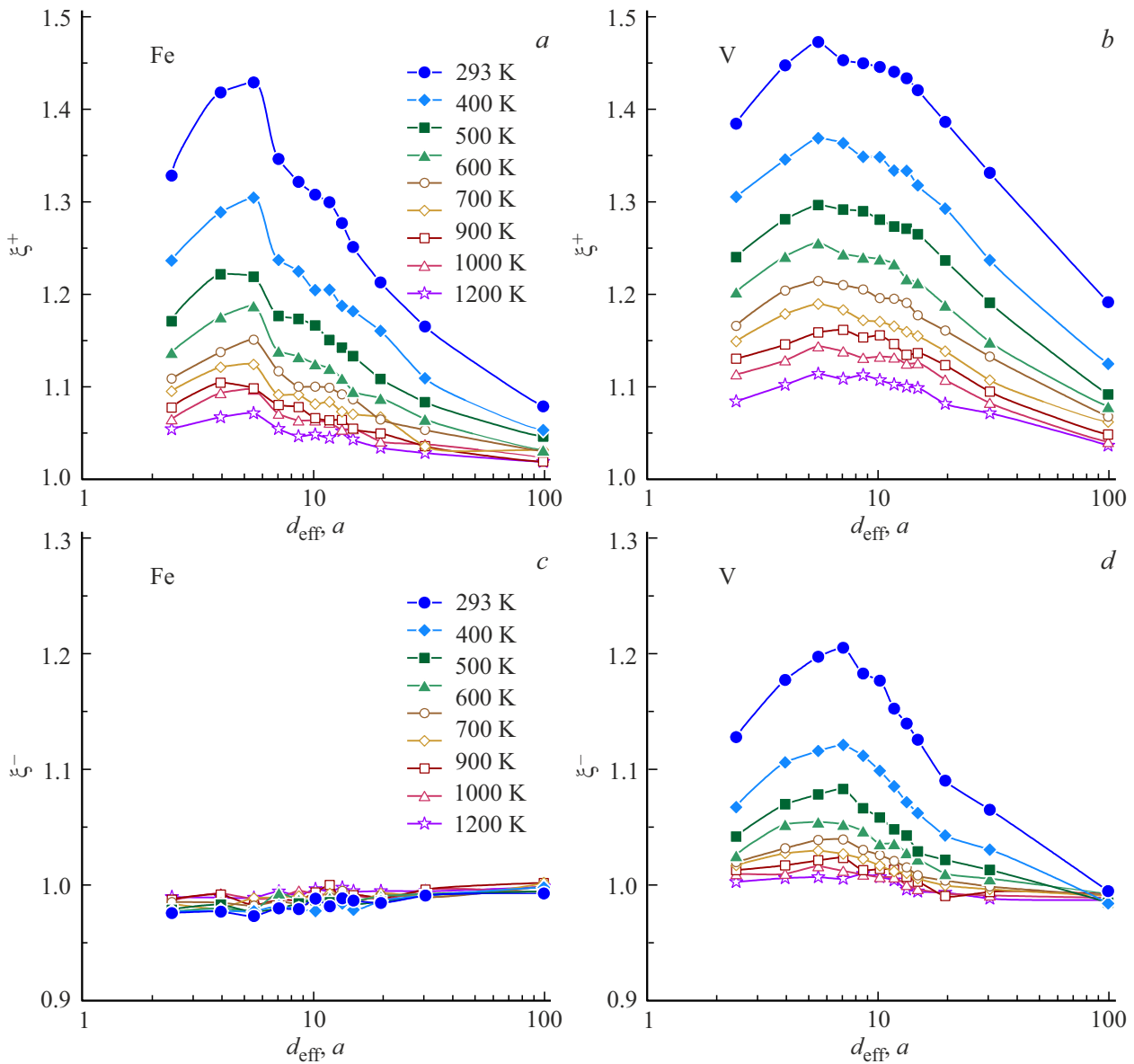


**Figure 4.** Size dependences of sink efficiencies of  $R_{110}$ -voids for SIAs (a, b) and vacancies (c, d) in Fe (a, c) and V (b, d).

–  $\lesssim 10\%$  for vacancies in Fe (it is difficult to determine more accurately because the deviation of  $\xi^-$  from 1 is small even when all terms of  $E$  are taken into account).

These results correlate well with the values of  $\text{Tr}P/(3P_n)$  listed in Table 6 (the higher the value the higher the effect of the first term of (8) on the void sink efficiency) because it can be seen from (8) that the relation between the first and second terms is proportional to  $\text{Tr}P/(3P_n)$ .

Figures 6 and 7 show the calculated dependences of the void bias factor on temperature and void size with  $N_V = (400a)^{-3}$  (void bias factor is essentially independent of void concentration). Statistical errors approximately correspond to the size of dots on the curves. Void bias factor at all  $T$  and  $d_{\text{eff}}$  is positive and decreases tending to zero as the temperature grows (Figure 6).  $D(d_{\text{eff}})$  first

grow with  $d_{\text{eff}}$  and reach their maximum with  $d_{\text{eff}} = 5.5a$  in Fe and  $d_{\text{eff}} = 10-20a$  in V (data scatter is caused by temperature) and then decrease tending to zero (Figure 7). For the smallest void ( $d_{\text{eff}} = 2.4a$ ),  $D$  varies with  $T$  from 15% to 2% in Fe and from 10% to 3% in V.

## 4. Discussion

A necessary condition for void growth in the traditional theory of radiation-induced swelling of metals [1–3] is that the void bias factor shall be lower than the dislocation bias factor ( $D_d > D_V$ ). Most of the dislocations in a material before irradiation are of screw type.  $D_d$  depends on the dislocation density  $\rho_d$  ( $D_d$  grows with  $\rho_d$  [37]) as opposed to  $D_V$  that is independent of  $N_V$  (due to a weak dependence

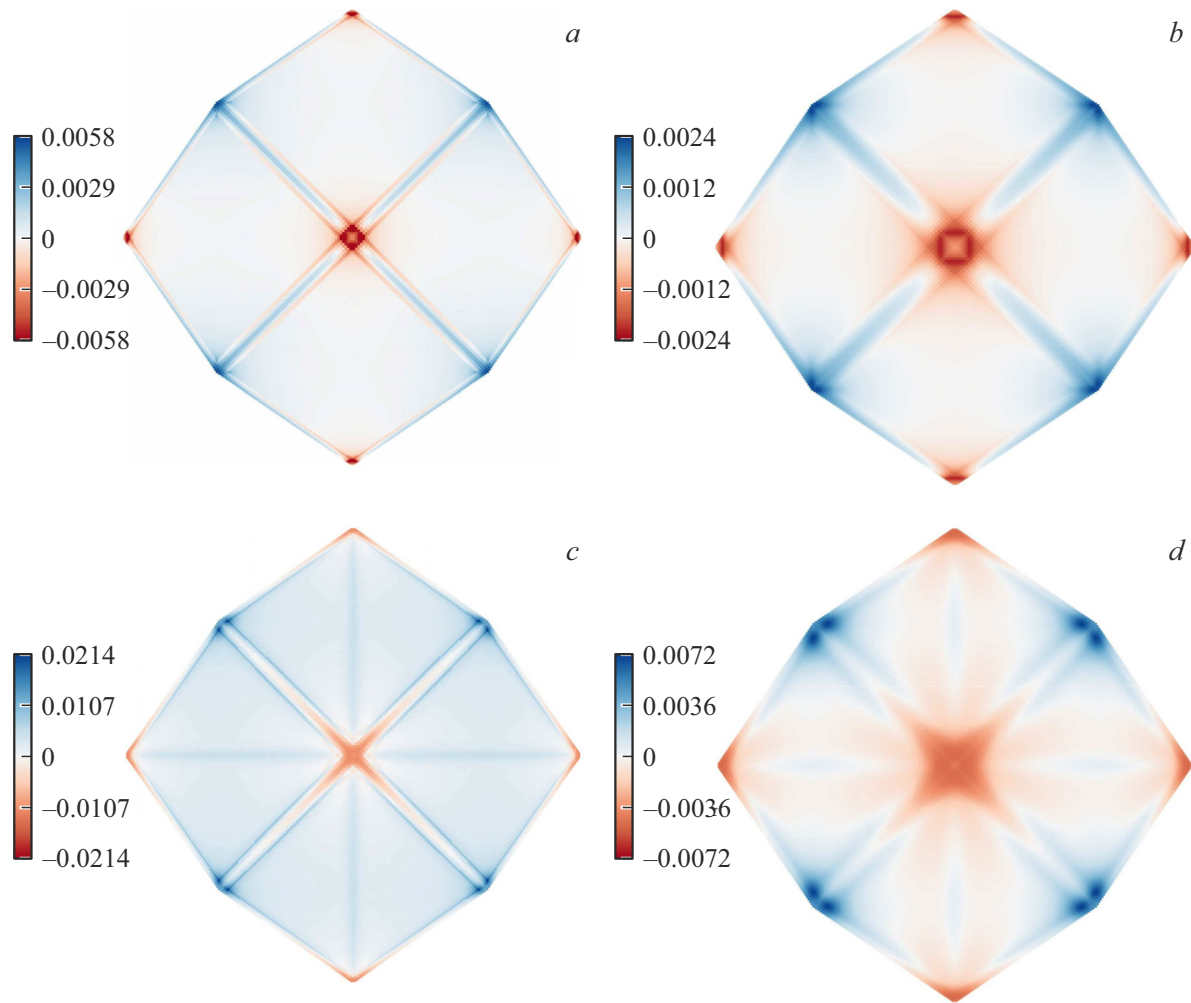


**Figure 5.** Distribution of volumetric strains in the 2-nd (*a,c*) and 5-th (*b,d*) monoatomic near-surface layers near the  $R_{110}$ -void with  $d_{\text{eff}} = 99a$  in Fe (*a,b*) and V (*c,d*).

**Table 6.**  $\text{Tr } P/3$ ,  $P_n$  and  $\text{Tr } P/(3P_n)$  for SPDs in Fe and V [19,27]

Metal	SPD	$\text{Tr } P/3$ , eV	$P_n$ , eV	$\text{Tr } P/(3P_n)$
Fe	Vacancy	-1.43	-1.68	0.85
	SIA	18.67	4.53	4.1
V	Vacancy	-6.11	-1.20	5.1
	SIA	17.11	1.29	13.3

of the sink efficiency of voids on  $N_V$  as mentioned at the beginning of Section 3.2). Figure 8 shows  $D_d(T)$  for screw dislocations with different  $\rho_d$  (from  $10^{11}$  to  $10^{15} \text{ m}^{-2}$ ) in Fe and V calculated according to the relations proposed in [37]. This figure also shows  $D_V(T)$  for voids with the smallest size ( $2.4a$ ) and voids with size  $5.5a$  in Fe and  $10-20a$  in V that have the maximum bias factor (see Figure 7).

Atomic collision cascades resulting from energy transfer from neutrons to crystal lattice atoms directly form void

nuclei. According to the MD simulation data concerning cascades in Fe and V with the damaging energy up to 50 keV in [38], it is shown that vacancy clusters containing less than 18 vacancies remain in the cascade region after its thermalization (times shorter than  $\sim 0.1$  ns). Such number of vacancies in the cluster corresponds approximately to the smallest  $R_{110}$ -void with size  $2.4a$  addressed in this work.

As one can see in Figure 8, a sufficiently high  $\rho_d$  at the irradiation start can ensure that  $D_d > D_V$  is met, which is necessary for the growth of void nuclei that are formed in atomic collision cascades. In this case, when the bias factor of growing voids reaches the maximum value  $D_{V,\text{max}}$  with  $d_{\text{eff}}$  equal to  $5.5a$  for Fe and  $10-20a$  (depending on  $T$ ) for V, respectively (Figure 8),  $D_V$  will gradually decrease to zero. Therefore, a decrease in  $\rho_d$  from the initial high value, which usually takes place during irradiation, will not affect the fulfilment of  $D_d > D_V$  for already grown voids and unlimited swelling will continue. There is no incubation period for swelling in this case.

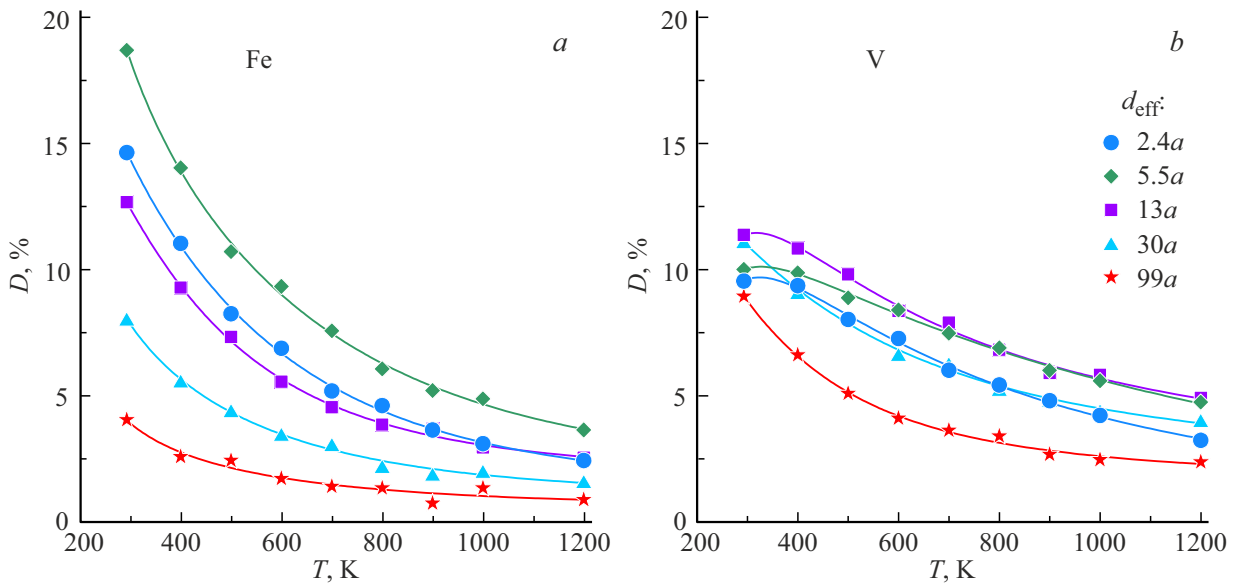


**Figure 6.** Temperature dependence of the  $R_{110}$ -void bias factor in Fe (a) and V (b). Solid lines — approximations on the basis of expressions (4), (7).

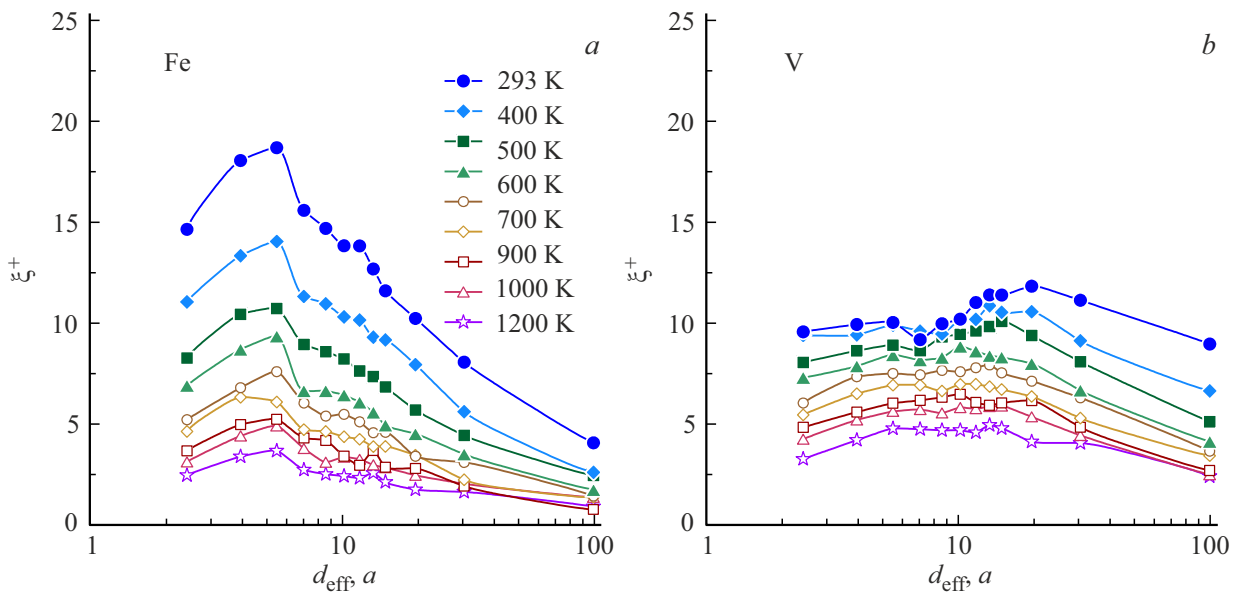


**Figure 7.** Size dependence of the  $R_{110}$ -void bias factor in Fe (a) and V (b).

If  $\rho_d$  is low enough (annealed material) to meet  $D_d < D_V$  for void nuclei, then void nuclei forming in the atomic collision cascades will be dissolved due to a prevailing SIA flux on them. Thus, if the dislocation bias factor doesn't increase during irradiation (due to the change of  $\rho_d$  and/or type of dislocations), the material will not swell. In this case, there will be an incubation period for swelling, duration of which depends on the stability of the initial dislocation microstructure.

If  $\rho_d$  is such as the dislocation bias factor is higher than the void nuclei bias factor, but lower than the maximum void bias factor  $D_{V,\text{max}}$ , then void nuclei that are formed in

cascades will grow until  $D_d = D_V$  is met, then these voids will stop growing because the vacancy and SIA flux on them will be equal to each other. The material will continue swelling due to continued formation of new void nuclei and growth of them to maximum permissible size. In such case, after irradiation, a high concentration of voids with relatively small size shall be observed, incubation period is absent.

Note that this conclusions were made on the basis of approximations used in the traditional theory of radiation-induced swelling of metals [1–3] (homogeneous effective medium containing uniformly distributed sinks [23]), and do not take into account possible spatial correlation effects,

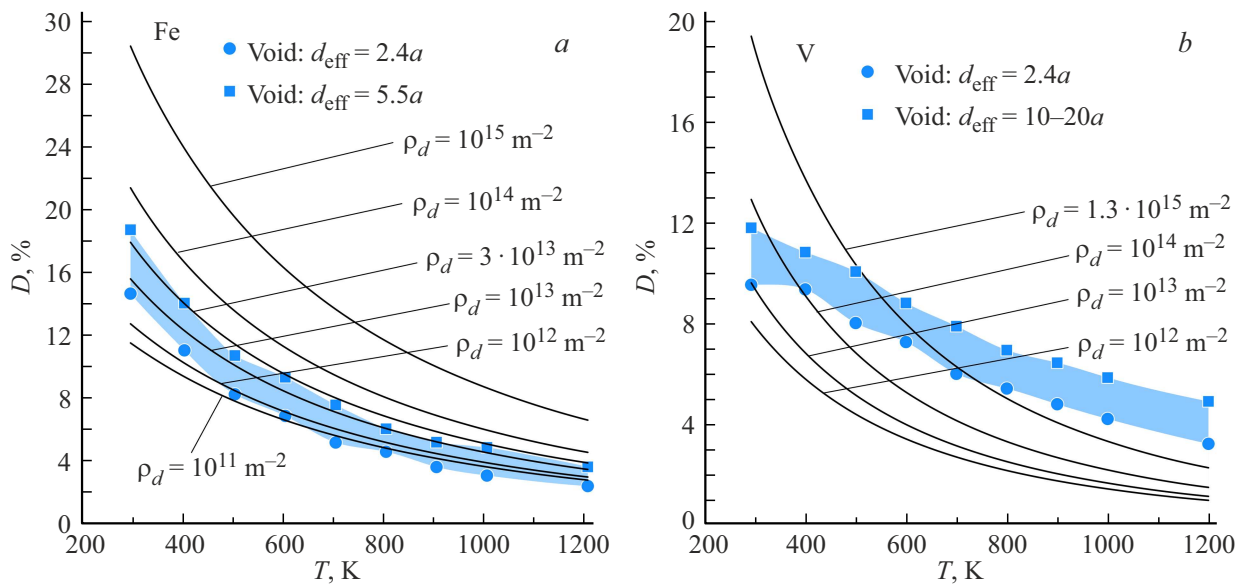


**Figure 8.** Temperature dependences of the bias factors of screw dislocations and voids with the smallest considered size ( $2.4a$ ) and the maximum bias factors of voids (void size  $5.5a$  for Fe and  $10-20a$  for V) in Fe (a) and V (b). A blue-filled area shows the values taken on by the bias factor of voids growing from  $2.4a$  to the above-mentioned sizes that correspond to the maximum preferences.

which may lead to local variation of bias factors and, consequently, the local microstructure evolution may differ from the general trend. Nevertheless, if voids are formed locally in the material, while the most of the bulk is free from voids, then the total void concentration will be low and, consequently, the macroscopic change of material volume will be small.

Let's compare the experimental data concerning the microstructure evolution of Fe and V with different initial microstructure in neutron irradiation conditions in fast reactors (the exposed samples were annealed or cold worked before irradiation). Irradiation results shall be preferably compared at similar (ideally identical) temperatures and damaging dose rates.

#### 4.1. Iron

In [39], cold worked (CW) and annealed samples were irradiated in the BR-10 reactor to 25.8 dpa at  $400^\circ\text{C}$  and dose rate of  $4 \cdot 10^{-7}$  dpa/s. Initial  $\rho_d$  of samples was  $1-2 \cdot 10^{15}$  and  $< 10^{13} \text{ m}^{-2}$ , respectively. After irradiation, these samples swelled by 4.5% ( $\langle d \rangle \sim 400a$ ) and 1.7% ( $\langle d \rangle \sim 200a$ ), respectively, contrary to widespread perception that cold working of a material can suppress swelling.

Similar comparison of data from [40,41] where a CW sample (BR-10 reactor,  $400^\circ\text{C}$ ,  $10^{-7}$  dpa/s, 6.2 dpa,  $\rho_d = 2.2 \cdot 10^{14} \text{ m}^{-2}$ ) and annealed sample (BOR-60 reactor,  $345^\circ\text{C}$ ,  $1.8 \cdot 10^{-7}$  dpa/s, 58 dpa, initial  $\rho_d$  is not available) shows that swelling also goes more rapidly in the CW material: 3% per 6.2 dpa ( $\langle d \rangle \sim 150a$ ) in the CW sample and 3.2% per 58 dpa in the annealed sample.

The listed experimental data for Fe fits into a picture drawn using the model data (Figure 8, a). In CW

samples with high initial  $\rho_d$ , the above-mentioned case is implemented, when  $D_d > D_V$ : swelling starts without an incubation period. In the annealed samples,  $D_d < D_V$  case is apparently implemented at the start of irradiation, which leads to a long incubation period during which no material swelling occurs. During irradiation of the annealed sample according to [39],  $\rho_d$  grows from  $< 10^{13}$  to  $3 \cdot 10^{13} \text{ m}^{-2}$ , thus,  $D_d > D_{V,\text{max}}$  is met and, consequently, swelling takes place.

#### 4.2. Vanadium

For vanadium in [42,43], it is shown that the annealed samples (initial  $\rho_d < 10^{12} \text{ m}^{-2}$ ) irradiated in the JOYO and FFTF reactors to 13.7 dpa and 34.2 dpa either do not swell at all or swell a little in the temperature range of  $400-600^\circ\text{C}$ . There are no voids at all during irradiation to 13.7 dpa in the JOYO reactor at  $400^\circ\text{C}$  and  $500^\circ\text{C}$ , and a limited amount of voids is observed at  $600^\circ\text{C}$  (swelling  $\sim 1.4\%$ ). Swelling to  $\sim 1\%$  is observed in the FFTF reactor: at  $410^\circ\text{C}$  and 31.5 dpa ( $\langle d \rangle \sim 14a$ ); at  $520^\circ\text{C}$  and 31.9 dpa ( $\langle d \rangle \sim 70a$ ); at  $600^\circ\text{C}$  and 34.2 dpa ( $\langle d \rangle \sim 160a$ ) ( $\langle d \rangle$  is the mean void size).

It is shown in [44] that V irradiated in the BR-10 reactor at  $370^\circ\text{C}$  and dose rate of  $2.5 \cdot 10^{-7}$  dpa/s to 1.3 dpa swells to 0.63% ( $\langle d \rangle \sim 15a$ ). Initial  $\rho_d$  in [44] was not measured, therefore, as the dose is not too high,  $\rho_d$  after irradiation equal to  $\sim 1.3 \cdot 10^{15} \text{ m}^{-2}$  will be used as reference.

The above-mentioned experimental data for vanadium also fits into the model approximations (Figure 8, b). In the annealed samples,  $D_d < D_V$  case is implemented at the start of irradiation due to low  $\rho_d$ , which leads to a long incubation period during which no material swelling occurs. In [44], a situation apparently takes place where  $D_d$  is higher

than the bias factor of small voids due to high  $\rho_d$ , but lower than the maximum void bias factor  $D_{V,max}$ , which leads to the start of swelling without an incubation period and to a high concentration of relatively small voids.

## 5. Conclusion

For BCC metals, Fe and V, the most energetically favorable void faceting has been established. Sink strengths of voids for self-point defects (vacancies, interstitial atoms) and bias factors (relative differences of sink strengths for interstitial atoms and vacancies) have been calculated.

1. Formation energies of voids with size  $2-100a$  and different faceting (cubes with the  $\{100\}$  facets, octahedra with the  $\{110\}$  facets, rhombic dodecahedra with the  $\{110\}$  facets, regular octahedra with the  $\{111\}$  facets, deltoidal icositetrahedra with the  $\{211\}$  facets, spheres) have been calculated by the molecular statics method for BCC metals, Fe and V. Surface energies of the free  $\{100\}$ ,  $\{110\}$ ,  $\{111\}$ ,  $\{211\}$  surfaces have been determined as asymptotes of size dependences of void formation energies in the limit of their large sizes. The  $\{110\}$  surface has the smallest surface energy. When voids are larger than  $2.4a$ , a rhombic dodecahedron with the  $\{110\}$  facets —  $R_{110}$  is the most energetically favorable void faceting type.

2. For  $R_{110}$ -voids in Fe and V, their sink strengths for SPDs and bias factors (void size range  $2.4-99a$  and temperature range  $293-1200$  K) have been calculated using the multiscale approach. Within this approach, the anisotropic SPD diffusion in void elastic fields determined by the MS method has been simulated by the OKMC method.

2.1. Void-induced volumetric and shear elastic strains are comparable with each other in magnitude as opposed to the commonly used Eshelby solution for void bias factor calculation for a spherical inclusion in an isotropic medium that is free from volumetric strains. Volumetric strains make a significant, and sometimes the main, contribution to formation of sink strengths and bias factors of voids in Fe and V.

2.2. Void bias factor decreases as the temperature grows. Size dependence of the void bias factor is non-monotonic. In the small void size range (from  $2.4a$ ), the bias factor grows as the void size increases and reaches its maximum values at  $5.5a$  in Fe and  $10-20a$  in V (a range of values is given for V because this size varies with temperature). Then, its values decrease and tend to zero. The void bias factor may take on values comparable in magnitude with the screw dislocation bias factor for voids smaller than several tens of  $a$ .

3. Within the traditional theory of radiation-induced swelling with parameters determined in this work, the features of void growth under neutron damaging irradiation conditions in Fe and V with different initial dislocation microstructures are considered. Calculation and theoretical data of this work explain the experimentally observed

radiation-induced swelling behavior of pure Fe and V exposed to neutron radiation in fast reactors.

## Funding

The study was carried out under the state assignment of the National Research Center „Kurchatov Institute“ using the equipment provided by the Shared Research Facility „Complex for Simulation and Processing of Mega-Class Research Facility Data“ NRC „Kurchatov Institute“ <http://ckp.nrcki.ru/>.

## Conflict of interest

The authors declare no conflict of interest.

## References

- [1] H. Wiedersich. *Radiat. Eff.* **12**, 1–2, 111 (1972). <https://doi.org/10.1080/00337577208231128>
- [2] S.I. Golubov, A.V. Barashev, R.E. Stoller. In: *Comprehensive Nuclear Materials* / Eds R.J.M. Konings, R.E. Stoller. 2 Ed. Elsevier, Amsterdam (2020). V. 1. P. 717. <https://doi.org/10.1016/B978-0-12-803581-8.00663-9>
- [3] V.V. Slezov, A.V. Subbotin, O.A. Osmaev. *Phys. Solid State* **47**, 3, 477 (2005). <https://doi.org/10.1134/1.1884708>
- [4] V.I. Dubinko, P.N. Ostapchuk, V.V. Slezov. *J. Nucl. Mater.* **161**, 2, 239 (1989). [https://doi.org/10.1016/0022-3115\(89\)90488-1](https://doi.org/10.1016/0022-3115(89)90488-1)
- [5] P.N. Ostapchuk. *Phys. Solid State* **54**, 1, 98 (2012). <https://doi.org/10.1134/S106378341201026X>
- [6] P.H. Dederichs, K. Schroeder. *Phys. Rev. B* **17**, 6, 2524 (1978). <https://doi.org/10.1103/PhysRevB.17.2524>
- [7] V.A. Borodin, A.I. Ryazanov, C. Abromeit. *J. Nucl. Mater.* **207**, 242 (1993). [https://doi.org/10.1016/0022-3115\(93\)90266-2](https://doi.org/10.1016/0022-3115(93)90266-2)
- [8] D. Carpentier, T. Jourdan, Y. Le Bouar, M.-C. Marinica. *Acta Mater.* **136**, 323 (2017). <https://doi.org/10.1016/j.actamat.2017.07.013>
- [9] S. Kaur, M. Athenes, J. Creuze. *J. Comp. Phys.* **454**, 110987 (2022). <https://doi.org/10.1016/j.jcp.2022.110987>
- [10] G.F.B. Moladje, L. Thuinet, C. Domain, C.S. Becquart, A. Legris. *Comput. Mater. Sci.* **183**, 109905 (2020). <https://doi.org/10.1016/j.commatsci.2020.109905>
- [11] J.D. Eshelby. *Proc. R. Soc. A* **241**, 1226, 376 (1957). <https://doi.org/10.1098/rspa.1957.0133>
- [12] J.D. Eshelby. *Proc. R. Soc. A* **252**, 1271, 561 (1959). <https://doi.org/10.1098/rspa.1959.0173>
- [13] A.V. Nazarov, A.A. Mikheev, A.P. Melnikov. *J. Nucl. Mater.* **532**, 152067 (2020). <https://doi.org/10.1016/j.jnucmat.2020.152067>
- [14] A.B. Sivak, P.A. Sivak. *Phys. Atom. Nuclei* **85**, 7, 1256 (2022). <https://doi.org/10.1134/S1063778822070183>
- [15] S.I. Golubov, Ye.N. Kaipetskaya. *Phys. Metals Metallogr.* **54**, 6, 16 (1982).
- [16] A.A. Kohnert, M.A. Cusentino, B.D. Wirth. *J. Nucl. Mater.* **499**, 480 (2018). <https://doi.org/10.1016/j.jnucmat.2017.12.005>
- [17] Y. Wang, F. Gao, B.D. Wirth. *J. Nucl. Mater.* **568**, 153882 (2022). <https://doi.org/10.1016/j.jnucmat.2022.153882>

- [18] V.M. Chernov, M.V. Leonteva-Smirnova, M.M. Potapenko, N.I. Budylkin, Yu.N. Devyatko, A.G. Ioltoukhovskiy, E.G. Mironova, A.K. Shikov, A.B. Sivak, G.N. Yermolaev. *Nucl. Fusion* **47**, 8, 839 (2007).  
<https://doi.org/10.1088/0029-5515/47/8/015>
- [19] A.B. Sivak, V.M. Chernov, V.A. Romanov, P.A. Sivak. *J. Nucl. Mater.* **417**, 1–3, 1067 (2011).  
<https://doi.org/10.1016/j.jnucmat.2010.12.176>
- [20] E. Gaudry. In: *Comprehensive Inorganic Chemistry III* / Eds J. Reedijk, K.R. Poeppelmeier. 3 Ed. Elsevier, Amsterdam (2023). V. 3. P. 74.  
<https://doi.org/10.1016/B978-0-12-823144-9.00134-5>
- [21] L. Malerba, M.C. Marinica, N. Anento, C. Björkas, H. Nguyen, C. Domain, F. Djurabekova, P. Olsson, K. Nordlund, A. Serra, D. Terentyev, F. Willaime, C.S. Becquart. *J. Nucl. Mater.* **406**, 1, 19 (2010).  
<https://doi.org/10.1016/j.jnucmat.2010.05.017>
- [22] M.I. Mendeleev, S. Han, W. Son, G.J. Ackland, D.J. Srolovitz. *Phys. Rev. B* **76**, 214105 (2007).  
<https://doi.org/10.1103/PhysRevB.76.214105>
- [23] A.D. Bailsford, R. Bulloch. *Phil. Trans. R. Soc. A.* **302**, 1465, 87 (1981). <https://doi.org/10.1098/rsta.1981.0158>
- [24] R.A. Johnson. *Phys. Rev.* **134**, 5A, A1329 (1964).  
<https://doi.org/10.1103/PhysRev.134.A1329>
- [25] E. Kröner. *Arch. Rational Mech. An.* **4**, 273 (1959/60).  
<https://doi.org/10.1007/BF00281393>
- [26] M.P. Puls, C.H. Woo. *J. Nucl. Mater.* **139**, 1, 48 (1986).  
[https://doi.org/10.1016/0022-3115\(86\)90163-7](https://doi.org/10.1016/0022-3115(86)90163-7)
- [27] A.B. Sivak, V.M. Chernov, N.A. Dubasova, V.A. Romanov. *J. Nucl. Mater.* **367–370**, 316 (2007).  
<https://doi.org/10.1016/j.jnucmat.2007.03.134>
- [28] A.B. Sivak, V.A. Romanov, D.N. Demidov, P.A. Sivak, V.M. Chernov, VANT, Ser. Materialovedenie i novye materialy **100**, 4, 5 (2019). (in Russian).  
<https://elibrary.ru/item.asp?id=44630370>
- [29] L. Malerba, C.S. Becquart, C. Domain. *J. Nucl. Mater.* **360**, 2, 159 (2007). <https://doi.org/10.1016/j.jnucmat.2006.10.002>
- [30] A.B. Sivak, P.A. Sivak, V.M. Chernov. *J. Nucl. Mater.* **531**, 152006 (2020). <https://doi.org/10.1016/j.jnucmat.2020.152006>
- [31] M. Methfessel, D. Hennig, M. Scheffler. *Phys. Rev. B* **46**, 8, 4816 (1992). <https://doi.org/10.1103/PhysRevB.46.4816>
- [32] C. Kittel. *Introduction to solid state physics*. 8 Ed. Wiley, New York (2005). 680 p.
- [33] S.J. Zinkle. In: *Comprehensive nuclear materials* / Ed R.J.M. Konings. Elsevier, Amsterdam (2012). V. 1. P. 65.  
<https://doi.org/10.1016/B978-0-08-056033-5.00003-3>
- [34] B.L. Eyre. *Proc. Int. Discussion Meeting on „Defects in refractory metals“*. Mol, Belgium (1972). P. 311.
- [35] A.F. Bartlett, J.H. Evans, B.L. Eyre, E.H. Terry, T.M. Williams. *Proc. Int. Conf. on „Radiation effects and tritium technology for fusion reactors“*. Gatlinburg, Tennessee, USA (1975). P. 122.
- [36] G.L. Kulcinski, B. Mastel, J.L. Brimhall. *Radiat. Eff.* **2**, 1, 57 (1969). <https://doi.org/10.1080/00337576908235581>
- [37] A.B. Sivak, P.A. Sivak, V.A. Romanov, V.M. Chernov. *Inorg. Mater. Appl. Res.* **6**, 2, 105 (2015).  
<https://doi.org/10.1134/S2075113315020161>
- [38] A.B. Sivak, D.N. Demidov, K.P. Zolnikov, A.V. Korchuganov, P.A. Sivak, V.A. Romanov, V.M. Chernov. VANT, ser. Materialovedenie i novye materialy **100**, 4, 25 (2019). (in Russian).  
<https://elibrary.ru/item.asp?id=44630371>
- [39] A.M. Dvoriashin, S.I. Porollo, Yu.V. Konobeev, F.A. Garner. *J. Nucl. Mater.* **283–287**, 157 (2000).  
[https://doi.org/10.1016/S0022-3115\(00\)00337-8](https://doi.org/10.1016/S0022-3115(00)00337-8)
- [40] S.I. Porollo, A.M. Dvoriashin, A.N. Vorobyev, Yu.V. Konobeev. *J. Nucl. Mater.* **256**, 247 (1998).  
[https://doi.org/10.1016/S0022-3115\(98\)00043-9](https://doi.org/10.1016/S0022-3115(98)00043-9)
- [41] N.I. Budylkin, E.G. Mironova, V.M. Chernov, V.A. Krasnoselov, S.I. Porollo, F.A. Garner. *J. Nucl. Mater.* **375**, 359 (2008). <https://doi.org/10.1016/j.jnucmat.2008.01.015>
- [42] H. Matsui, H. Nakajima, S. Yoshida. *J. Nucl. Mater.* **205**, 452 (1993). [https://doi.org/10.1016/0022-3115\(93\)90109-C](https://doi.org/10.1016/0022-3115(93)90109-C)
- [43] H. Nakajima, S. Yoshida, Y. Kohno, H. Matsui. *J. Nucl. Mater.*, **191–194**, 952 (1992).  
[https://doi.org/10.1016/0022-3115\(92\)90614-Q](https://doi.org/10.1016/0022-3115(92)90614-Q)
- [44] S.I. Porollo, A.M. Dvoriashin, Yu.V. Konobeev. *Phys. Metals Metallogr.* **123**, 8, 784 (2022).  
<https://doi.org/10.1134/S0031918X22080075>

*Translated by E.Ilinskaya*